Quantification of microstructure in a eutectic high entropy alloy AlCoCrFeNi2.1

PAPER • **OPEN ACCESS**

Quantification of microstructure in a eutectic high entropy alloy $AlCoCrFeNi_{2.1}$

To cite this article: Adrianna Lozinko *et al* 2019 *IOP Conf. Ser.: Mater. Sci. Eng.* **580** 012039

IOP Conf. Series: Materials Science and Engineering **580** (2019) 012039 doi:10.1088/1757-899X/580/1/012039

Quantification of microstructure in a eutectic high entropy alloy $AlCoCrFeNi_{2.1}$

Adrianna Lozinko [1], Oleg V. Mishin [2], Tianbo Yu [2], Uta Klement [1], Sheng Guo [1], Yubin Zhang [2*]

[1]Department of Industrial and Materials Science, Chalmers University of Technology, SE-412 96 Gothenburg, Sweden
[2] Department of Mechanical Engineering, Technical University of Denmark, DK 2800 Kgs. Lyngby, Denmark

Email: yubz@mek.dtu.dk

Abstract. Eutectic high entropy alloys (EHEAs) are a new class of metallic alloys with good mechanical properties at various temperatures. In the present investigation, microstructural parameters such as the volume fraction of two phases (FCC ($L1_2$) and BCC (B2)) forming the eutectic, the orientation relationship between these phases and interphase boundary spacings in as-cast EHEA $AlCoCrFeNi_{2.1}$ were quantified using electron microscopy. It is found that the two phases have a Kurdjumov-Sachs orientation relationship, i.e., $\{111\}_{FCC} \parallel \{110\}_{BCC}$ and $\langle 110\rangle_{FCC} \parallel \langle 111\rangle_{BCC}$. It is also found that both regular semi-coherent lamellar and irregular curved interphase boundaries are present within individual eutectic colonies. The habit planes for the semi-coherent lamellar interfaces are {224} and {123} for the FCC and BCC phases, respectively. Quantitative microstructural analysis shows that the ratio of volume fractions of the FCC and BCC phases within the regular lamellar regions differs to that within irregular regions, which suggests a local chemistry difference between the two regions. Finally, the solidification process of EHEAs is discussed, and possible ways to optimize the mechanical properties by microstructural design are suggested.

1. Introduction

High entropy alloys (HEAs), also known as multi-principal-element alloys, became well-known firstly in 2004 [1,2], and have now become new research frontier in the field of metallic alloys. HEAs contain at least four principal elements, which are often mixed in equiatomic or close to equiatomic ratios. HEAs open up a massive and unexplored compositional space, beyond that previously defined by traditional alloy design strategies, leading to the development of novel metallic materials with unprecedented structural and functional properties. For example, exceptional fracture toughness was revealed in a CoCrFeMnNi alloy at cryogenic temperatures [3], and some metastable high-entropy dual-phase alloys were observed to overcome the strength-ductility trade-off [4]. Additionally, novel multicomponent nanoparticles for catalysis [5], new superconducting materials [6], and even superhard ceramic materials [7] have been obtained based on the HEA concept.

Recently, a new class of metallic alloys, eutectic HEAs (EHEAs) has been developed, containing a mixture of the BCC and FCC phases. These alloys demonstrate high strength and ductility up to 700 °C [8]. Among the EHEAs that have been developed so far, the first proposed EHEA, $AlCoCrFeNi_{2.1}$, has attracted the most attention [9–11]. However, a detailed description of the

microstructure has still not been provided, and the solidification process for this alloy is still poorly understood.

In the present study, the microstructure of this $AlCoCrFeNi_{2.1}$ EHEA is characterized using scanning electron microscopy (SEM), electron backscatter diffraction (EBSD), and transmission electron microscopy (TEM). Microstructural parameters, including the spatial distribution and volume fractions of the phases, and the spacing and habit plane of the semi-coherent interphase boundaries are quantified. The quantitative description of the microstructure provides a better understanding of the solidification process as well as a link to account for the mechanical properties. The results obtained are essential for developing advanced computer models for improved design of HEAs.

2. Experimental

The $AlCoCrFeNi_{2.1}$ (elements in atomic ratios) alloy was prepared through an arc melting route, using high purity (> 99.9 %) metals, in a Ti-gettered high-purity argon atmosphere. Melting was repeated at least five times on flipped samples to improve the homogeneity of the ingot. Finally, the ingot was suction-cast into a copper mold with $10 \times 10 \times 60$ mm^3 dimensions.

The crystal structure and phases were characterized by X-ray diffraction, using a Bruker AXS D8 Advance diffractometer with Cr-Kα radiation, operated at 35 kV with a beam current of 50 mA. The scanning range was 35 – 158 °, with a 0.025 ° step size and a scanning speed of 0.15 °/min.

Samples were mechanically polished using standard polishing suspensions, with particle sizes down to 1 μm, followed by chemical polishing using an OP-S solution. SEM and EBSD analysis were performed with a Zeiss Leo Gemini 1550 field emission gun scanning electron microscope. For EBSD, an acceleration voltage of 20 kV and a step size of 75 nm were used. For TEM observations, a thin foil was prepared by twin-jet electrochemical polishing in a 1:3 $HClO_4$:C_2H_5OH solution at 0 °C and 12 V. The foil was investigated in a JEOL 2100 microscope.

3. Results

3.1. Microstructural characterization

EBSD maps and TEM images showing the microstructure of the EHEA are given in figure 1. A very complex structure is seen in the EBSD map. The microstructure consists of ordered FCC ($L1_2$) and ordered BCC (B2) phases, shown in figure 1a in red and blue, respectively. The volume fractions of the FCC and BCC phases are about 69% and 31%, respectively. The lattice parameters determined from X-ray diffraction are 0.3590 nm for the FCC phase and 0.2873 nm for the BCC phase.

Two distinct features are seen within individual eutectic colonies: regular lamellae with straight interphase boundaries; and fragmented regions with irregular curved boundaries (see figure 1a-c). The lamellae are in most cases connected to the colony boundaries at both sides (see the white lines in figure 1a), while the irregular curved boundaries tend to be aligned perpendicular to the lamellar boundaries (see e.g. the regions marked by the yellow arrows in figure 1a and 1b). Each lamellar bundle consists of typically four to six thin lamellae of each phase, and some of the lamellae can be 60 μm long. Serrations or jogs also appear in the lamellar regions. In some cases, the long lamellae are interrupted, especially for the BCC phase (see e.g. the one marked by the white arrow in figure 1a).

Twin boundaries are seen within the FCC phase, highlighted in green in figure 1a. Most colonies contain only one set of straight interphase boundaries, while a few colonies containing twin variants can have multiple sets of straight interphase boundaries (see e.g. the colony A in figure 1a). Misfit dislocations are present along the straight interphase boundaries, i.e., these interfaces are semi-coherent (see figure 1c).

Microstructural quantification based on the EBSD maps indicates that the volume fractions of the lamellar and irregular regions are about 42% and 58%, respectively (see table 1). The relative volume fraction of the FCC phase is slightly higher in the irregular regions ($42/58 \approx 72\%$) than in the regular lamellar regions ($29/42 \approx 69\%$). The average width of the well-defined lamellae is finer than the average width within the irregular regions for both phases (see table 1). There is also a difference in

the interphase boundary spacing between the FCC and BCC phases: the former is roughly twice the latter.

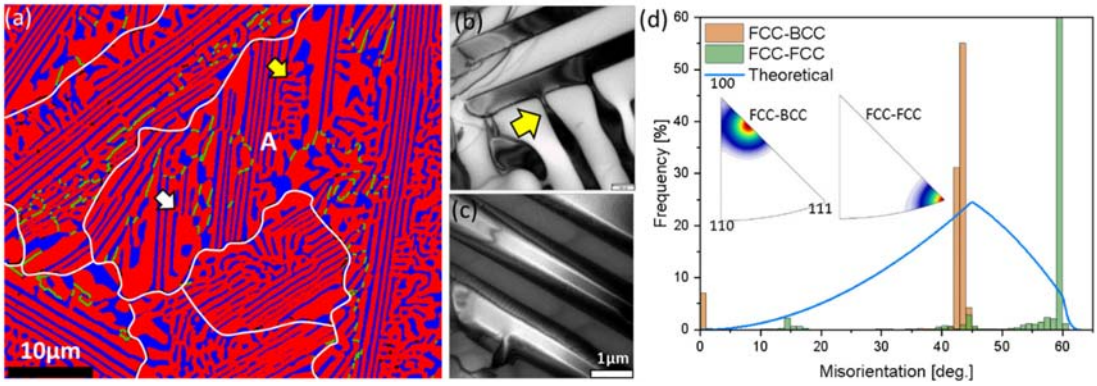

Figure 1. Microstructure of the as-cast $AlCoCrFeNi_{2.1}$ EHEA. (a) EBSD phase map, where the FCC and BCC phases are shown in red and blue, respectively. FCC twin boundaries are shown in green, while the white lines mark the eutectic colony boundaries. (b) and (c) TEM images. Semi-coherent straight interphase boundaries with misfit dislocations are seen in (c). (d) misorientation (angle-axis pair) distribution for interphase boundaries for boundaries within the FCC phase. The white and yellow arrows in (a) and (b) mark an interrupted BCC lamella and dendrite-like features, respectively.

Table 1. Microstructural parameters for the FCC and BCC phases in two regions with different morphologies in the EBSD map in figure 1a.

Phase	Lamellar region		Irregular region	
	Average width (μm)	Phase fraction (%)	Average width (μm)	Phase fraction (%)
FCC	0.70	29	1.16	42
BCC	0.35	13	0.59	16
All	-	42	-	58

In spite of the fragmented structure within the colonies, all the fragments have a nearly identical crystallographic orientation for the BCC phase, and similarly nearly identical for the FCC except for one twin variant (see e.g. figure 2a-c). The misorientation between the BCC and FCC phases within each colony is about 43°⟨114⟩ (see figure 1d). From the pole figures for the two phases in figure 2b and 2c, it can be seen that one {111} plane in the FCC phase for each twin is parallel to one {110} plane in the BCC phase, and similarly one {110} plane in the FCC phase is parallel to one {111} plane in the BCC phase. This corresponds to the well-known Kurdjumov-Sachs (K-S) orientation relationship, and this relationship is observed for both lamellar and irregular regions.

To determine the crystallographic plane for the straight interphase boundaries, Kikuchi diffraction patterns of the two phases in a colony were recorded in using TEM. As shown in figure 3, when the interface is edge-on, the {112} and {224} planes of the FCC phase and the {123} plane of the BCC phase are almost parallel to the interphase boundary traces. This result is further supported by the analysis based on the EBSD and SEM data (see figure 2d and 2e).

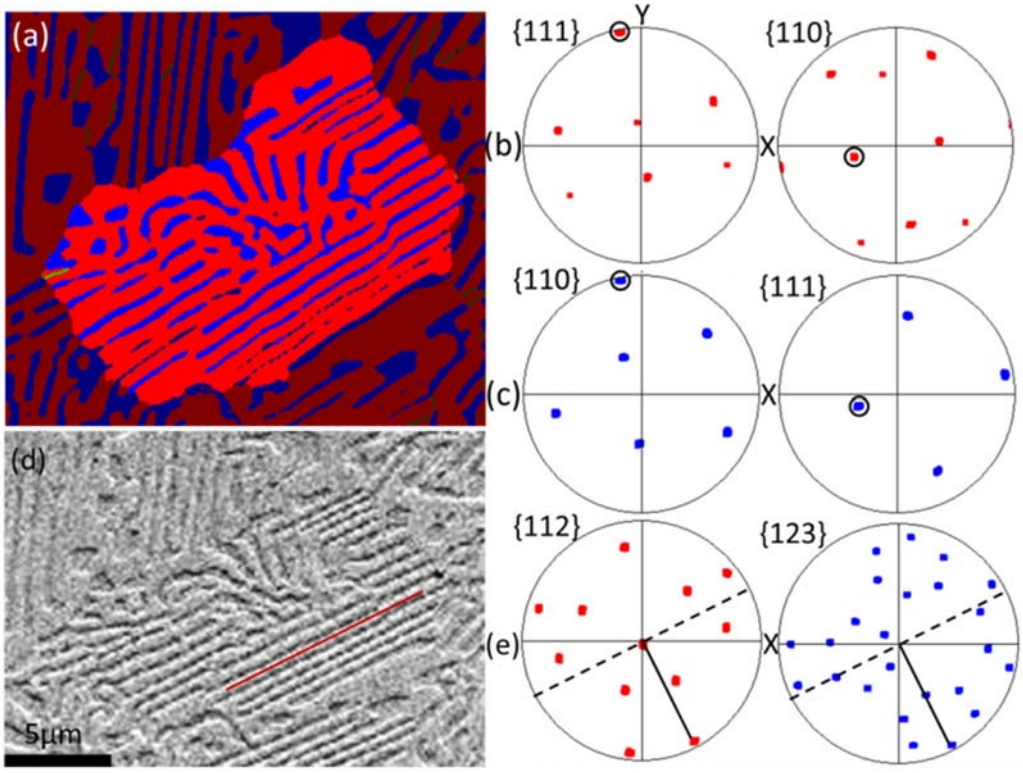

Figure 2. Analysis of orientation relationship between the FCC and BCC phases. (a) EBSD phase map for one highlighted colony, where the FCC and BCC phases are shown in red and blue, respectively. FCC twin boundaries are shown in green. (b) and (c) {111} and {110} pole figures showing the orientation relationship between the FCC and BCC phases. (d) SEM image taken in the same region as in (a). (e) {112} and {123} pole figures for the FCC and BCC phases, respectively, showing the crystallographic plane that is parallel to the lamellae direction (marked by the red line in (d)). Pole figures with red and blue colours are from FCC and BCC phases, respectively.

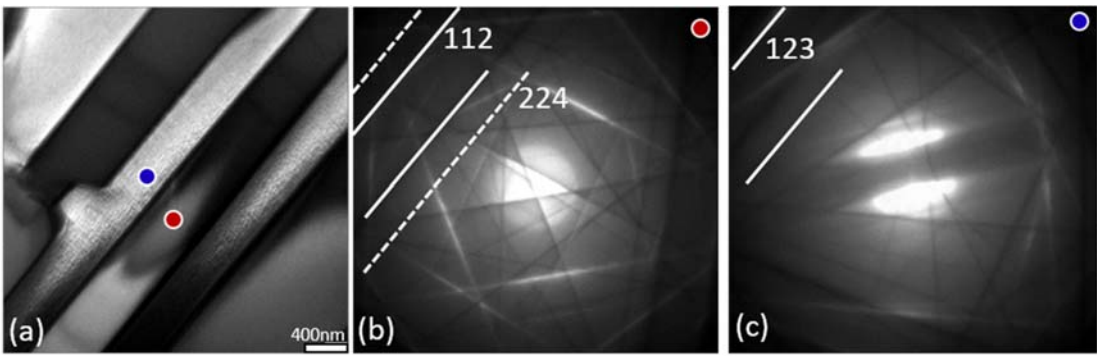

Figure 3. TEM analysis of interphase boundaries in a lamellar region: (a) TEM image, where red and blue dots mark FCC and BCC lamellae, respectively. (b) and (c) are Kikuchi patterns from the FCC and BCC lamellae, respectively. It is seen that the Kikuchi lines are parallel to the straight interface in (a).

4. Discussion

In the present EHEA alloy, the FCC and BCC phases form cooperatively during solidification. Based on different types of eutectic reactions, a distinction has been made between *normal* and *anomalous* eutectic alloys. *Normal* alloys are distinguished by well-defined lamellar structures and orientation relationships, while *anomalous* alloys show typically an irregular structure with no preferred orientation relationship [12]. The present results show that there is a clear orientation relationship between the two phases in $AlCoCrFeNi_{2.1}$. Therefore, it is concluded that this EHEA is a *normal* eutectic alloy. The two phases have a Kurdjumov-Sachs orientation relationship, i.e., $\{111\}_{FCC} \parallel \{110\}_{BCC}$ and $\langle 110\rangle_{FCC} \parallel \langle 111\rangle_{BCC}$, which agrees with the conclusions of Ref. [13].

The TEM analysis shows the presence of semi-coherent interphase boundaries, and that these boundaries are parallel to the FCC {112}/{224} planes and BCC {123} planes (see figure 3). The lattice plane spacings for the FCC {224} and BCC {123} planes are quite similar, 0.0733 nm and 0.0768 nm, respectively. The habit planes are therefore likely to be {224} and {123} for the FCC and BCC phases, respectively. The misfit between the two planes is about 5%, which leads to the formation of misfit dislocations to accommodate the misfit strain (see figure 1c).

The results also show that the irregular regions develop on both sides of the lamellar regions. It is suggested that the irregular structure is typically formed because the growth rates of the two phases are different: one phase solidifies faster than the other phase. For the present case, the FCC phase solidifies faster than the BCC phase, leading to the formation of local dendrite-like structures along the BCC lamellae (see figures 1a and 1b) and to the formation of the interrupted BCC lamellae. Additionally, a higher volume fraction of the FCC phase can contribute to the formation of the irregular structure [12]. For volume fractions of the FCC and BCC phases in the irregular regions of greater than 2:1, the balance for the cooperative growth between FCC and BCC with the expected volume fraction ratio of 2:1 can be broken.

Based on the observed results, the solidification process of the $AlCoCrFeNi_{2.1}$ EHEA can be briefly described as follows:

i. The two phases nucleate and grow cooperatively along the low energy semi-coherent interfaces (habit plane). The volume fraction ratio between the FCC and BCC phase is 2:1.
ii. During solidification, the FCC phase grows faster than the BCC phase, leading to the formation of interrupted lamellae and dendrite-like structures in the BCC phase.
iii. Stacking faults can occur in the FCC phase, which leads to the formation of twins predominantly perpendicular to the lamellar direction (see figure 1a).

Based on the present results, it cannot be concluded how the local chemical segregation affects the growth of the two phases. Assuming that the chemical content of the FCC and BCC phases in the regular and irregular regions is identical, the higher FCC fraction in the irregular regions implies local chemical segregation, i.e., more elements that compose the FCC phase segregate in the liquid and form a higher fraction of this phase in the irregular regions. Further experimental characterization of the local chemistry and simulations such as phase field modeling are required to understand this process.

From the materials design point of view, lamellar structures with coherent/semi-coherent boundaries can be beneficial for mechanical properties [14], as the lamellae typically deform cooperatively, which significantly increases the strength. On the other hand, the low energy structure of the coherent or semi-coherent boundaries can absorb more dislocations, which can improve material ductility. In addition, flat interphase boundaries are usually extraordinarily stable at elevated temperatures because of the low energy structure and lack of capillary driving force for migration. In contrast, the non-coherent interphase boundaries can be expected to behave like conventional grain boundaries with less stability at high temperatures. For the present alloy, the average interphase boundary spacing for the irregular regions is larger than that for the lamellar regions, implying that the strength in the irregular regions is lower than that of the lamellar regions. Apparently, to improve mechanical properties, the processing should be optimized to eliminate the formation of the irregular regions. Two possible ways are proposed here:

i. To change the chemical composition according to the chemistry in the lamellar regions, so that chemical segregation will not occur during the eutectic reaction and only the lamellar structure will be formed during the eutectic reaction.
ii. To increase the cooling rate in order to suppress the local segregation and to refine the lamellar boundary spacing, which can significantly improve the mechanical properties.

5. Conclusions

In the present paper, the microstructure of the as-cast eutectic high entropy alloy $AlCoCrFeNi_{2.1}$ has been quantified in detail using electron microscopy. The results show that this alloy consists of two phases, FCC and BCC, with volume fractions of 69% and 31%, respectively. Within individual eutectic colonies, the microstructure can be divided into two regions with distinct features: a regular lamellar structure in the center and an irregular structure on both sides of the lamellar region. The orientation relationship for these two types of structures is however identical, and is described by the Kurdjumov-Sachs orientation relationship, i.e., $\{111\}_{FCC} \parallel \{110\}_{BCC}$ and $\langle 110\rangle_{FCC} \parallel \langle 111\rangle_{BCC}$. The habit planes for the lamellar interfaces are determined to be {224} and {123} for the FCC and BCC phases, respectively. Microstructural analysis shows that the ratio of the volume fractions of the FCC and BCC phases is higher in the irregular regions than in the lamellar regions. This suggests that local chemical segregation is more likely to occur during the solidification process, which can be the main reason for the development of the irregular regions.

Acknowledgements

AL and SG thank the financial support from the Swedish Research Council (2015-04087). The authors acknowledge additional funding from InterReg. TY and YZ thank further the financial support by the European Research Council (ERC) under the European Union's Horizon 2020 research and innovation programme (M4D – grant agreement No. 788567).

References

[1] Yeh J W, Chen S K, Lin S J, Gan J Y, Chin T S, Shun T T, Tsau C H and Chang S Y 2004 *Adv. Eng. Mater.* **6** 299–303
[2] Cantor B, Chang I T H, Knight P and Vincent A J B 2004 *Mater. Sci. Eng. A* **375**–**377** 213–8
[3] Gludovatz B, Hohenwarter A, Catoor D, Chang E H, George E P and Ritchie R O 2014 *Science.* **345** 1153–8
[4] Li Z, Pradeep K G, Deng Y, Raabe D and Tasan C C 2016 *Nature* **534** 227-30
[5] Yao Y, Huang Z, Xie P, Lacey S D, Jacob R J, Xie H, Chen F, Nie A, Pu T, Rehwoldt M, Yu D, Zachariah M R, Wang C, Shahbazian-Yassar R, Li J and Hu L 2018 *Science.* **359** 1489–94
[6] Koželj P, Vrtnik S, Jelen A, Jazbec S, Jagličić Z, Maiti S, Feuerbacher M, Steurer W and Dolinšek J 2014 *Phys. Rev. Lett.* **113** 1–5
[7] Sarker P, Harrington T, Toher C, Oses C, Samiee M, Maria J P, Brenner D W, Vecchio K S and Curtarolo S 2018 *Nat. Commun.* **9** 1–10
[8] Lu Y, Dong Y, Guo S, Jiang L, Kang H, Wang T, Wen B, Wang Z, Jie J, Cao Z, Ruan H and Li T 2014 *Sci. Rep.* **4** 6200
[9] Lu Y, Jiang H, Guo S, Wang T, Cao Z and Li T 2017 *Intermetallics* **91** 124–8
[10] Wani I S, Bhattacharjee T, Sheikh S, Bhattacharjee P P, Guo S and Tsuji N 2016 *Mater. Sci. Eng. A* **675** 99–109
[11] Shi P, Ren W, Zheng T, Ren Z, Hou X, Peng J, Hu P, Gao Y, Zhong Y and Liaw P K 2019 *Nat. Commun.* **10** 1–8
[12] Glicksman M E 2011 *Principles of Solidification: An Introduction to Modern Casting and Crystal Growth Concepts* (New York, NY: Springer New York)
[13] Wang Q, Lu Y, Yu Q and Zhang Z 2018 *Sci. Rep.* **8** 14910
[14] Lu K, Lu K, Lu L and Suresh S 2009 *Science.* **349** 349–53